Journal of Materials Chemistry A

PAPER

View Article Online
View Journal | View Issue

Cite this: J. Mater. Chem. A, 2015, 3, 13507

Facile synthesis of microcellular foam catalysts with adjustable hierarchical porous structure, acid–base strength and wettability for biomass energy conversion†

Heping Gao,[ab] Jianming Pan,*[a] Donglai Han,[c] Yunlei Zhang,[a] Weidong Shi,[a] Jun Zeng,[b] Yinxian Peng*[b] and Yongsheng Yan[a]

Herein we report a novel synthetic strategy for fabrication of microcellular foam catalysts (MFCs) with hydrophobic, acid–base, and hierarchical porous properties for conversion of one-pot cellulose to a key chemical platform (*i.e.* 5-hydroxymethylfurfural, HMF) for biofuels. The water-in-oil (W/O) Pickering high internal phase emulsions (HIPEs), stabilized by both amino-functionalized nanoparticles (namely, S-NH_2) and Span 80, were used as the template for simultaneous polymerization of oil phase containing 1-octene, divinylbenzene (DVB), and trihydroxymethylpropyl trimethylacrylate (TMPTMA). After subsequent sulfonation process, acid and base sites resulting from grafted $-SO_3H$ group of polydivinylbenzene (PDVB) and S-NH_2 were both located on the surface of the MFCs. The resultant MFCs composite had a typical hierarchical porous structure, and the macropores with a well-defined open-cell and interconnecting pore throat structure could be controlled *via* the composition of the oil phase of emulsion, with the mesopore structure closely related to the degree of cross-linking of oil-soluble functional monomer. The representative catalyst MFCs-3 had a hierarchical porous structure (macropores ranging from 1.0 μm to 30 μm and uniform mesopores in 32.1 nm), hydrophobic surface (water contact angle of 125°), 0.735 mmol g^{-1} of base, and 1.305 mmol g^{-1} of acid. The HMF yield of 41% for cellulose conversion showed its excellent catalytic performance. This work opens up a route for simple and controlled fabrication of multifunctional polymeric catalysts for biomass energy conversion.

Received 27th March 2015
Accepted 18th May 2015

DOI: 10.1039/c5ta02239h

www.rsc.org/MaterialsA

1 Introduction

Increasing concern about global warming and declining reserves of easily accessible, non-renewable fossil fuels have resulted in growth of development of clean and sustainable resources such as chemical feedstocks. Abundant renewable biomass derived mainly from photosynthetic processes of plants, capable of producing both energy and organic compounds with many applications, has the most potential as a sustainable source to replace fossil fuels.[1–3] Thus, there is much interest in effective conversion of cellulose, a non-edible component of biomass, to high value-added chemicals. 5-Hydroxymethylfurfural (HMF) derived from cellulosic biomass has a potential leading role in bio-based energy, because HMF can be converted into many versatile and multifunctional compounds such as 5-hydroxy-4-keto-2-pentenoic acid,[4] the promising fuel 2,5-dimethylfuran,[5–7] and other organic derivatives.[8–10] Among many methods for production of HMF, acid-catalyzed dehydration of C_6-based carbohydrates has the broadest perspective for applications to relieve the energy crisis. Within acid catalyst systems, heterogeneous acid catalysts, with advantages including low corrosion of equipment, high catalytic activity and recyclability, simple handling requirements, and environmentally friendly nature, have gradually replaced the traditional corrosive and hazardous homogeneous acid catalysts, such as HCl, H_2SO_4, $HClO_4$, and H_3PO_4.[11–13]

Recently, various solid acid catalysts have been produced and applied in catalysis of cellulose into HMF. For example, Lanzafame *et al.* successfully synthesized sulfated zirconia solid acid catalyst supported over mesoporous silica (SBA-15) using a hydrolysis method, and HMF was obtained by catalyzing cellulose to HMF at 190 °C in water solution.[14] In our previous work, we used a water-in-oil (W/O) Pickering high internal phase emulsions (HIPEs) template to prepare macroporous polymerized solid acid with an open-cell structure, interconnecting

[a]School of Chemistry and Chemical Engineering, Jiangsu University, Zhenjiang 212013, China. E-mail: zhenjiangpjm@126.com; Fax: +86 88791800; Tel: +86 88791708

[b]School of Environmental and Chemical Engineering, Jiangsu University of Science and Technology, Zhenjiang 212003, China

[c]Changchun Institute of Optics, Fine Mechanics and Physics, Chinese Academy of Sciences, Changchun 130033, China

† Electronic supplementary information (ESI) available. See DOI: 10.1039/c5ta02239h

pores and strong acidity, and then the polymerized solid acid was used to convert cellulose into HMF. We also overcame the shortcoming of mesoporous catalysts, in that it is difficult to diffuse large molecules (*e.g.* cellulose) into the mesopores.[15] We applied precipitation polymerization and polymerization in Pickering emulsion, combined with a sulfonation process to synthesize two kinds of polymeric solid acid for converting cellulose to HMF.[16] Although these catalysts showed obvious availability in one-pot cellulose to HMF conversion, the main problem of improving the HMF yield from cellulose remains a serious challenge in this field.

In recent years, huge efforts have been focused on how to improve the HMF yield from C_6-based carbohydrates. The concept for rational design and synthesis of the solid acid catalyst is based on the following important facts. Firstly, it is commonly accepted that most solid acid catalysts are deactivated or decomposed by water produced as a byproduct or added to the reaction system, because water co-adsorbed on the surface of the catalyst produces a more hydrophilic interface.[17,18] HMF can be easily degraded into other products in the hydrophilic acid system, giving a low HMF yield. Recently, Xiao's group synthesized a series of acidic mesoporous polymeric catalysts with excellent hydrophobicity by copolymerization of divinylbenzene and sodium *p*-styrene sulfonate, and a high HMF yield (>99.0%) was achieved using such a hydrophobic acid catalyst with fructose.[19] Secondly, the proposed mechanism of cellulose conversion to HMF involves three main reactions: (1) cellulose to glucose depolymerization in the presence of an acid catalyst, (2) glucose to fructose isomerization using a base catalyst, and (3) fructose to HMF dehydration by an acid catalyst. Wu *et al.* successfully synthesized acid–base bi-functionalized mesoporous silica nanoparticles for one-pot conversion of cellulose to HMF in an ionic liquid system, and it was found that an acid–base bi-functionalized solid catalyst could significantly elevate the HMF yield from cellulose.[20] Thirdly, mesoporous catalysts exhibit excellent catalytic activity in various kinds of catalytic reaction because of their high specific surface areas.[21,22] Meanwhile, the main shortcomings of mesoporous catalysts, such as extra isolation steps required for catalyst recycling and slow mass transfer to active sites on the internal surface, can be overcame using hierarchical porous (*i.e.* meso-/macropores) polymeric catalysts.[23,24] Catalysts with hydrophobic and acid–base characteristics, and hierarchical porous structure (meso-/macropores) would efficiently improve HMF yield from cellulose, but obtaining such multifunctional polymeric solid catalysts remains a serious challenge.

In summary, a series of microcellular foam catalysts (MFCs) with hydrophobic, acid–base and hierarchical porous properties were successfully designed and synthesized using a W/O Pickering HIPEs template method and subsequent sulfonation process (Scheme 1). Firstly, both as-prepared hydrophobic amino-functionalized nanoparticles (namely, S-NH_2) and span 80 were used to stabilize W/O Pickering HIPEs with an internal phase volume ratio of 84.8%. Then, Pickering HIPEs of external oil phase containing 1-octene, trihydroxymethylpropyl trimethylacrylate (TMPTMA) and divinyl benzene (DVB) monomer, and internal phase comprising K_2SO_4 aqueous solution, were applied to fabricated porous polymeric materials. After sulfonation in 98% H_2SO_4, MFCs were obtained *via* grafting $-SO_3H$ groups onto polydivinylbenzene (PDVB). The amounts of base and acid were controlled by adjusting the contents of S-NH_2 and DVB monomer, respectively, and various wettabilities of MFCs were obtained by changing the volume of 1-octene. The obtained MFCs were characterized, and their catalytic activities explored in detail by optimizing the reaction time, temperature and catalyst loading amounts in catalysis of cellulose to HMF.

2 Material and methods

2.1 Materials

The chemicals, 1-ethyl-3-methyl-imidazolium chloride ([EMIM]-Cl), cellulose (powder, *ca.* 50 micron), 5-hydroxymethylfurfural (HMF, >99%), trihydroxymethylpropyl trimethylacrylate (TMPTMA, 98%), styrene (St, 99.9%), divinylbenzene (DVB, 80%), glycidyl methacrylate (GMA, 97%), *N*,*N*-dimethylformamide (DMF, 99.8%), hexadecane (>99%) and tetrahydrofuran (THF, 99.9%) were supplied by Aladdin reagent CO., LTD (Shanghai, China). Fluorescein isothiocyanate (FITC), 2,2′-azobis (2-methyl-propionitrile) (AIBN, 99%), ethanol, methanol, Span 80, K_2SO_4, potassium persulfate (KPS), $NH_3 \cdot H_2O$ (25 wt%), and acetone were purchased from Sinopharm Chemical Reagent Co., Ltd. (Shanghai, China). All other chemicals were purchased from local suppliers and used without further purification.

2.2 Synthesis of S-NH_2 as stabilizer

S-NH_2 was synthesized *via* two steps using a slightly modified method.[25] Firstly, a few epoxy-bearing polymerized St nanoparticles (*i.e.* S-GMA) were prepared using a surfactant-free emulsion polymerization reaction. In a typical run, 0.6 mL of GMA and 50 mL of deionized water were placed in a 250 mL three-neck, round-bottom flask, and deoxygenated by putting nitrogen gas into the solution for 10 min under stirring, before 2.0 mL of St and 1.0 mL of DVB were added into the flask. Then, the mixture was heated to 90 °C in an oil bath, and 80 mg of the initiator KPS pre-dissolved in 10 mL of deionized water was added to the flask. The solution was left to react for 3.0 h under nitrogen protection. Subsequently, the reaction products were collected and washed by centrifugation several times with DMF, THF and ethanol, respectively. Finally, uniformly sized S-GMA was obtained through drying for 24 h at 40 °C in a vacuum drying oven.

Secondly, as-prepared S-GMA was further modified by $NH_3 \cdot H_2O$. As a typical run, S-GMA (0.5 g) and $NH_3 \cdot H_2O$ (10 mL) were mixed and stirred at 60 °C for 9.0 h in a 50 mL flask with a reflux condenser. Subsequently, the reaction products were separated and washed by centrifugation with ethanol several times. Finally, S-NH_2 was gained through drying for 12 h at 40 °C in a vacuum drying oven.

2.3 Fabrication of MFCs

MFCs were prepared by polymerization reaction and subsequent sulfonation process. The first step was fabrication and

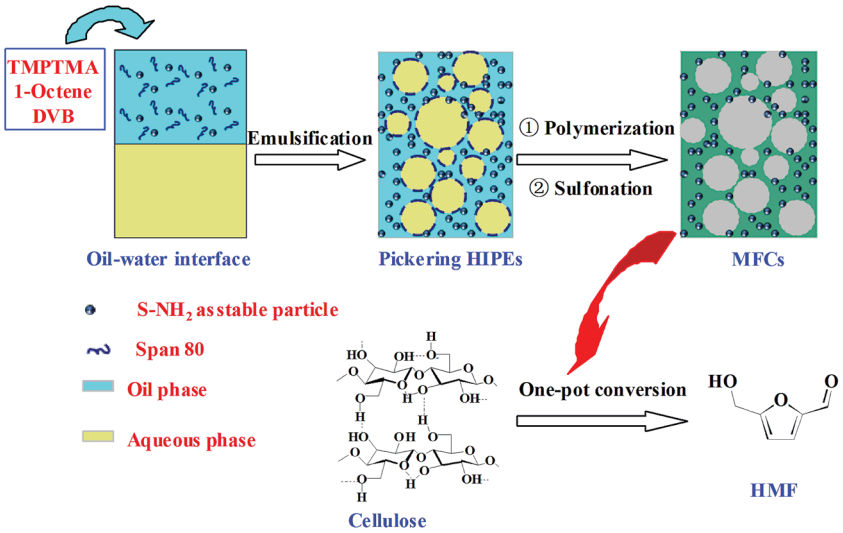

Scheme 1 Synthesis of MFCs and conversion of cellulose into HMF in [Emim]Cl under atmospheric pressure.

polymerization of stable W/O Pickering HIPEs (the HIPEs recipes are listed in Table 1). Firstly, the aqueous phase, containing K_2SO_4, was dropped into the organic phase (which was formed by stirring a mixture of TMPTMA, 1-octene, DVB, AIBN, S-NH_2 and Span80 in a 100 mL three-neck flask) under fast and continuous mechanical stirring with a digital display electric blender at 400 rpm for over 10 min, and stable W/O Pickering HIPEs were obtained. Secondly, the obtained Pickering HIPEs were transferred into a plastic centrifuge tube and polymerized in a circulating air oven at 70 °C for 12 h. Then, as-prepared polymerized HIPEs monoliths were washed with deionized water and acetone in turn by Soxhlet extraction, and further dried at 80 °C for 12 h in a vacuum oven, until a constant weight was achieved.

The second step was to graft the above monoliths with $-SO_3H$ groups by a sulfonation process. Briefly, polymerized HIPEs monoliths (1.0 g, column diameter was 2.6 cm) and 98% H_2SO_4 (30 mL) were mixed and stirred continuously at room temperature for 12 h. The products were filtered and washed to remove excess H_2SO_4 using deionized water. Finally, MFCs were obtained after drying in a vacuum at 80 °C for 3.0 h, and to adapt the experimental conditions, the big MFCs monoliths were further grinded to powder.

2.4 Conversion of cellulose to HMF and analysis of HMF

A typical procedure was used for conversion of cellulose to HMF according to modified Huang's method.[26] Firstly, cellulose (0.1 g) and [EMIM]Cl (2.0 g) were heated at 130 °C for 30 min under stirring until a clear solution formed, to destroy the degree of crystallization and regularity of the cellulose (Fig. S1a†). Then, as-prepared representative catalyst MFCs-3 powders (40 mg) were added to the mixed solution, and continued to react at 130 °C for 20 min under continuous stirring (Fig. S1b†). Next, the reaction products were quenched immediately with cold water, and diluted 5000 times with deionized water. Finally, liquid samples were analyzed by a high performance liquid chromatography (HPLC) with Agilent 1200. HMF was detected with a UV-Vis detector at a wavelength of 283 nm. An Agilent TC-C18 column (4.6 × 250 mm, 5.0 mm) was used. The mobile phase was mixed water and methanol with a volume ratio of 30 : 70, and the flow rate and column oven were set to 0.7 mL min^{-1} and 25 °C. Meanwhile, the HMF content was obtained according to the standard curve method. In this work, the HMF yield was defined as the ratio of total mole number of carbon atoms of HMF (n_1) and total mole number of carbon atoms in initial cellulose loaded in the reactor (n_0), as expressed in eqn (1).

Table 1 Recipes of W/O Pickering HIPEs

	External organic phase						Internal aqueous phase	
Samples	TMPTMA (mL)	1-Octene (mL)	DVB (mL)	AIBN (g)	S-NH_2 (g)	Span80 (mL)	Water (mL)	K_2SO_4 (g)
MFCs-1	0	1.0	2.0	0.05	0.3	0. 3	16.8	0.08
MFCs-2	0.5	2.0	0.5	0.05	0.3	0. 3	16.8	0.08
MFCs-3	0.8	2.0	0.2	0.05	0.3	0. 3	16.8	0.08
MFCs-4	0.8	2.0	0.2	0.05	0	0. 3	16.8	0.08

$$Y_{HMF}(\%) = 100 \times (n_1/n_0) \quad (1)$$

2.5 Instruments and characterization

A confocal laser scanning microscope (CLSM, Leica, TCSSP5II, Germany) was used for fluorescence testing. Optical micrographs of Pickering HIPEs were obtained using a DMM-330C optical microscope equipped with a high performance digital camera (CAIKON, China). The organic functional groups of MFCs were characterized using solid-state NMR spectroscopy (Bruker DSX-400WBNMR spectrometer, NMR/Solid 400). Electrospray ionization mass spectrometry (ESI-MS) was measured by liquid chromatography-ion trap mass spectrometry (Thermo LXQ, U.S.A.). FT-IR spectra were measured by Nicolet NEXUS-470 FTIR apparatus (U.S.A.). The morphology of the nanoparticles and MFCs were characterized by field emission scanning electron microscopy (SEM, JSM-7100F). XPS spectra were performed on a Thermo ESCALAB 250 with Al Kα radiation at y = 901 for the X-ray sources, the binding energies were calibrated using the C 1s peak at 284.9 eV. Elemental composition was recorded by the vario EL III elemental analyzer (Elementar, Hanau, Germany). The acidic and basic features of samples were both measured according to NH_3 temperature-programmed desorption (NH_3-TPD) and CO_2 temperature-programmed desorption (CO_2-TPD) curves, which were recorded using a thermal conductivity detector (TCD, DAS-7000, Beijing, China). TGA of samples was performed for powder (near 10 mg) using Diamond TG/DTA instrument (PerkinElmer, U.S.A.) under a nitrogen atmosphere up to 800 °C with a heating rate of 5.0 °C min^{-1}. The water contact angles of samples were measured using an Optical Contact Angle Measuring Device (KSV CM200): 2.0 μL of deionized water was injected onto the sample surface through the syringe pump, and then images of the water droplet were obtained using the camera in the measuring device about 30 s after the droplet had formed on the sample surface. The images were analyzed using the supplied software to determine the contact angle of the sample.

3 Results and discussion

3.1 Morphology of stable nanoparticles and hierarchical porous structure of catalysts

Catalytic amination of epoxy nanoparticles was the main technique used to produce basic particles with $-NH_2$ functional groups. SEM images of the S-GMA (a) and S-NH_2 (b) samples are presented in Fig. 1. The S-GMA nanoparticles (Fig. 1a) were clearly uniform with a size of 128 ± 2.0 nm. After amination, the size of the S-NH_2 (Fig. 1b) particles increased to 131 ± 2.0 nm, indirectly indicating successful grafting of the amino groups.

In general, particle-stabilized (surfactant-free) HIPEs templates are termed Pickering HIPEs. In some special cases, such as continuous phase of emulsion including unstable polymerized monomer, open porous polymeric materials can be synthesized from Pickering HIPEs.[27–30] However, in most cases, Pickering HIPEs produce closed-cell macroporous polymers with large pores.[31] Conventional polyHIPEs, synthesized from surfactant-stabilized HIPEs only, have poor mechanical properties and low permeabilities.[32–35] Thus, novel polyHIPEs have been synthesized with open porous structure and greatly enhanced permeability, by exploiting both particles and polymeric surfactant-stabilized HIPEs. The fabricated HIPEs systems employing polymeric surfactants as well as particles were also termed Pickering HIPEs in previous studies.[36] This may be because the particles were the primary stabilizer of the HIPEs in the presence of low polymeric surfactant.[36] In this study, MFCs were synthesized by polymerizing water-in-oil (W/O) Pickering HIPEs stabilized by Span 80 in combination with S-NH_2 particles; SEM images of MFCs-1 (c), MFCs-2 (d), MFCs-3 (e), and MFCs-4 (f) are presented in Fig. 1. All MFCs possessed controllable macropores with well-defined, open-cell and interconnecting pore throat structures, but the MFCs differed in terms of size and detailed macroporous structure. MFCs-1 had a void size of 15 ± 5.0 μm of the open-cell and a few interconnecting pore throats of 3.0 ± 2.0 μm. The open-cell (15 ± 7.0 μm) and a large number of small interconnecting pore throats (1.0 ± 0.5 μm) were observed in the case of MFCs-2 (Fig. 1d). An open-cell structure (void size of 20 ± 10 μm) with a large number of big interconnecting pore throats with sizes in the range of 1.0–5.0 μm were observed in the case of MFCs-3 (Fig. 1e). Based on the slight differences in open-cell structures, it can be concluded that the pore-cell size of the MFCs can be controlled based on the composition of the oil phase, except for the inner volume fraction of the emulsions, and the emulsion was extremely stable during the polymerization process. However, the sizes of the interconnecting pore throats were obviously different; the differences in the mode of pore throat

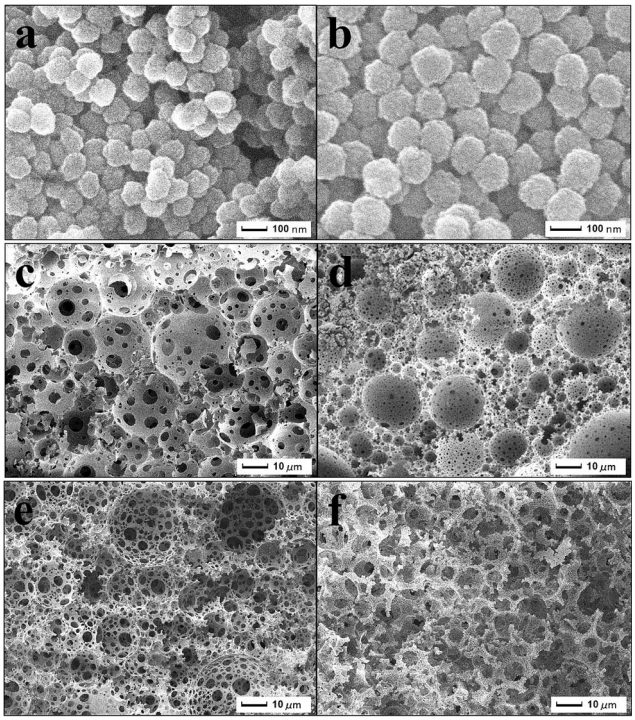

Fig. 1 SEM images of S-GMA (a), S-NH_2 (b), MFCs-1 (c), MFCs-2 (d), MFCs-3 (e), and MFCs-4 (f).

formation may arise as follows: (1) sufficiently thin films formed at the gap between two water–oil interfaces stabilized by the same surfactant (*i.e.* Span 80) to separate the droplets in the HIPEs may be easily broken to form interconnecting pore throats of the MFCs during the polymerization process.[37] (2) Generally, with the use of less TMPTMA cross-linker and DVB, less volume contraction occurs on conversion of the monomer to the polymer. Thus, the lower degree of cross-linking between TMPTMA and DVB in MFCs-3 led to a looser polymer structure, and window formation occurred because of volume contraction on conversion of the monomer to the polymer, which was favourable for formation of bigger interconnecting pore throats (1.0–5.0 μm) during copolymerization.[38] (3) The excess 1-octene in the case of MFCs-3, derived from the low conversion rate of polymerization, may function as a pore-forming reagent. The spatial effect of the long chain of these molecules and the low degree of cross-linking between TMPTMA and DVB in MFCs-3 limited self-polymerization to form a polymer-network, and simultaneous removal of low molecular weight 1-octene by Soxhlet extraction was relatively facile; thus, the pore-forming reagent derived from the functional monomer may facilitate formation of large interconnecting pore throats. Additionally, to estimate the effect of Span 80 and S-NH_2 on the structure of the catalyst, MFCs-4 with many broken open-cells (20 ± 5.0 μm) and interconnecting pore throats (5.0 ± 2.0 μm) was produced by polymerization of the surfactant-stabilized HIPEs. The loose nature of MFCs-4 corroborates the affirmation that the poor mechanical properties of the conventional W/O HIPE-templating porous polymers is caused by the presence of a large amount of non-ionic surfactant during the emulsifying process.[39] Although the non-ionic surfactant Span 80, which is known to be a suitable stabilizer for high internal phase emulsions, was employed for preparation of the HIPEs, and the MFCs-4 sample demonstrates that the HIPEs can be stabilized solely by Span 80, in our previous study,[40] it was demonstrated that the particles (S-NH_2) acted as the primary stabilizer of the Pickering HIPEs in the presence of this surfactant. Furthermore, the functionalized S-NH_2 particles generated polymerization "nodes", thereby increasing the cross-linking of the polymeric scaffold, and offered more active sites to form the tight structure of the catalyst during polymerization. Thus, the firm mechanical properties of MFCs-1, 2, and 3 are attributed to the presence of a large number of functionalized S-NH_2 particles compared with MFCs-4.

Mesopores in the structure have a remarkable effect on the catalytic efficacy.[41] The nitrogen adsorption–desorption isotherms and the size distribution curves of MFCs-1 (a), MFCs-2 (b), MFCs-3 (c), and MFCs-4 (d) are shown in Fig. 2. Typical type-IV isotherms with step capillary condensation in the relative pressure range of 0.1–0.9 were obtained for all samples, and this type of isotherm confirms the existence of mesopores. The porous parameters of MFCs-1, MFCs-2, MFCs-3, and MFCs-4 are listed in Table 2. The Brunauer–Emmett–Teller (BET) surface area (183.6 $m^2\ g^{-1}$) and pore volume (0.32 $cm^3\ g^{-1}$) of MFCs-1 were obviously higher than those of MFCs-2 (108.4 $m^2\ g^{-1}$, 0.24 $cm^3\ g^{-1}$), MFCs-3 (14.6 $m^2\ g^{-1}$, 0.05 $cm^3\ g^{-1}$), and MFCs-4 (3.5 $m^2\ g^{-1}$, 0.01 $cm^3\ g^{-1}$). However, the Barrett–Joyner–Halenda (BJH) mean pore diameter (8.8 nm) of MFCs-1 was lower than that of MFCs-2 (10.7 nm), MFCs-3 (32.1 nm), and MFCs-4 (47.3 nm). Interestingly, the highly permeable MFCs were characterized by a lower surface area and pore volume, a larger BJH mean pore diameter, and a wider size distribution range. This is attributed to the low degree of cross-linking reducing the tightness of the network, with consequent formation of a mesoporous structure. In short, the typical hierarchical porous structure of the microcellular polymer foams was confirmed from the SEM and nitrogen adsorption–desorption isotherm analyses and the size distribution curves of the MFCs. Furthermore, it is confirmed that the size distribution of the MFCs is wide, from the nm level to the μm level. According to previous research, only mesopores larger than 20 nm in the catalyst act as conductive zones for cellulose conversion.[42–44] Thus, the as-prepared MFC catalysts that possess a microcellular structure and hierarchical porous character were suitable for conversion of cellulose to HMF. Herein, a high HMF yield could be obtained by catalyzing the dehydration of cellulose to HMF over the MFCs (*vide infra*).

The typical process for fabrication of MFCs-3 is shown in Fig. 3. Firstly, to estimate the mean droplet size, a drop of the Pickering HIPEs was placed on a microscope slide and viewed using an optical microscope. The droplets possessed typical HIPE morphology with spherical and polydisperse characteristics (Fig. 3a). A CLSM was employed to determine the type of emulsion. FITC, a fluorescent substance, was dissolved in the oil phase prior to formation of the emulsion, and it was deduced that the obtained emulsions were W/O Pickering HIPEs (Fig. S2†). The droplet size (about 20 μm) was close to that of the open-cell of MFCs-3 (Fig. 3a and S2†), where the open-cell of MFCs-3 originated from the void left by removal of the inner salt water droplet, which suggests that the cell formed in the polymerization process was stable. After sulfonation, light red monoliths (density: 0.158 g cm^{-3}, Fig. 3c) were obtained from the white polymerized HIPEs monoliths (density: 0.148 g cm^{-3}, Fig. 3b). The results suggest that MFCs-3 had the advantages of a low density, stable structure, and that $-SO_3H$ groups could be grafted successfully onto the polymerized HIPE monoliths based on analysis of the density and colour of the monoliths.

3.2 Wettability properties of the stable particles and the catalysts

To understand the wettability properties of the stable particles and the catalysts, water contact angle images were acquired as shown in Fig. 4a. The water contact angles of S-GMA and S-NH_2 were about 140° and 121°, respectively, suggesting that amino groups were successfully grafted onto the surface of S-GMA *via* ring opening of the epoxy group. The water contact angle of 121° perfectly satisfies the requirements for stabilizing the W/O Pickering HIPEs.[45] Moreover, the wettability differed for the various MFCs (*i.e.*, water contact angle = 20° for MFCs-1, 103° for MFCs-2, 125° for MFCs-3, and 98° for MFCs-4), where the wettability could be controlled effectively by varying the amounts of DVB and 1-octene. The lower the content of DVB

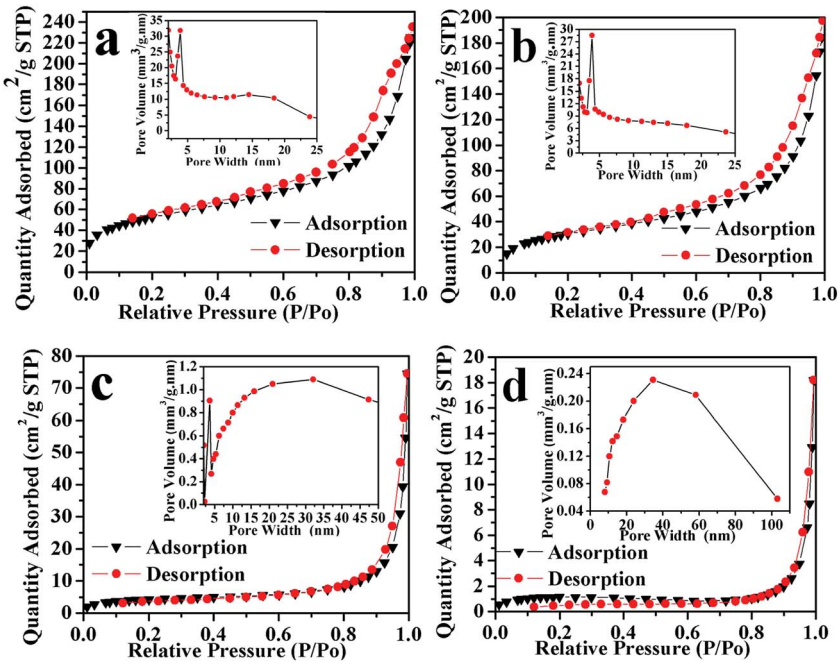

Fig. 2 Nitrogen adsorption–desorption isotherms of MFCs-1 (inset: pore distribution) (a), MFCs-2 (inset: pore distribution) (b), MFCs-3 (inset: pore distribution) (c), and MFCs-4 (inset: pore distribution) (d).

Table 2 Porosity properties of the catalysts

Samples	V_t[a] (cm^3 g^{-1})	D_{BJH}[b] (nm)	S_{BET}[c] (m^2 g^{-1})
MFCs-1	0.32	8.8	183.6
MFCs-2	0.24	10.7	108.4
MFCs-3	0.05	32.1	14.6
MFCs-4	0.01	47.3	3.5

[a] V_t is the total pore volume determined at the relative pressure of 0.99. [b] D_{BJH} is BJH mean pore diameter calculated by the desorption branches of the nitrogen sorption isotherms. [c] S_{BET} is the BET specific surface area.

utilized, the more hydrophobic the surface of the MFCs, which indicates that a higher content of DVB monomers produced more hydrophilic –SO_3H groups during the sulfonation process. Increasing the content of the 1-octene monomer was beneficial for increasing the hydrophobicity of the catalyst. Thus, adjusting the volume of DVB and 1-octene is an effective and simple approach for manipulating the wettability of the catalyst.

3.3 Chemical composition of the catalysts

The chemical composition of the stable particles and the catalysts was further analyzed based on elemental, ^{13}C CP/MAS NMR, FT-IR, X-ray photoelectron spectroscopy (XPS) analyses, and thermogravimetric analysis-differential scanning calorimetry (TG-DSC). The elemental compositions of the samples are shown in Fig. 4b. N was present in S-NH_2, MFCs-1, MFCs-2, and MFCs-3, and the mass percentages of N and S in the MFCs (5.8% S for MFCs-1, 6.1% S for MFCs-2, 6.77% S for MFCs-3, and 6.2% S for MFCs-4; 1.3% N for MFCs-1, 1.22% N for MFCs-2, and 1.03% N for MFCs-3) were slightly different. This was possibly because of the uneven distribution of S-NH_2 in MFCs and the different sulfonation contents of DVB required to graft the –SO_3H groups onto the surface of MFCs. Moreover, N was not detected in S-GMA and MFCs-4, suggesting that N was derived from the amination reaction of S-GMA with the epoxy groups, and the stable particles of S-NH_2 were retained in the MFCs after polymerization and sulfonation. The condensed structural formulas of S-NH_2 and MFCs-3 (Fig. 5a) were determined according to the ^{13}C CP/MAS NMR spectrum measurements,

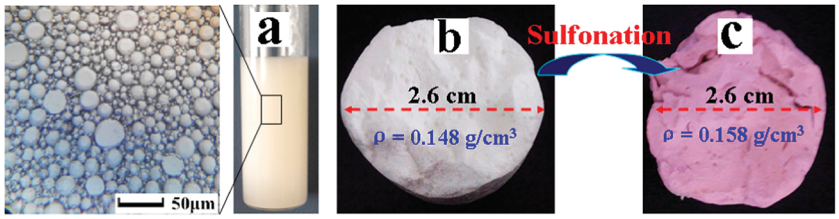

Fig. 3 Photos of Pickering HIPEs (a), polymerized HIPEs monoliths (b), and monoliths (c) of MFCs-3.

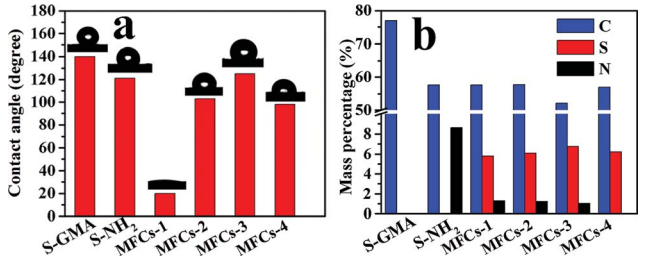

Fig. 4 Water contact angle measurements (a), element contents (b) of the stable nanoparticles and the catalysts.

meanwhile, the presence of S and N in the MFCs confirmed the success of the sulfonation and amination processes, respectively. The signal was detected at $d = 45.4$ ppm assigned to the carbon atoms bonded to amine groups (Fig. 5b and c) in the ^{13}C CP/MAS NMR spectra of both MFCs-3 and S-NH_2.[46] Another signal was detected at $d = 137.3$ ppm, assigned to the carbon atoms of a benzene ring bonded to –SO_3H groups in the ^{13}C CP/MAS NMR spectrum of MFCs-3. This observation confirms the presence of amine and sulfonic acid groups.

Fig. S3† shows the FT-IR spectra of MFCs-3 (a), MFCs-1 (b), MFCs-4 (c), MFCs-2 (d), S-GMA (e), and S-NH_2 (f). Peaks at 1456 cm^{-1} associated with the benzene ring could be clearly observed for all samples,[47] indicating the presence of the PDVB component. Additionally, peaks around 1033 cm^{-1}, attributed to the C–S bond, and at 1162 cm^{-1} (assigned to the –SO_3H group) also were clearly observed for the MFCs, indicating that the –SO_3H groups were successfully grafted onto the benzene rings of the PDVB component. Moreover, a peak at 1630 cm^{-1} assigned to –NH_2 groups was observed for all samples except for MFCs-4 and S-GMA, and peaks around 907 cm^{-1}, attributed to the epoxy groups, were apparent in the spectra of all samples, which indicate that –NH_2 groups were successfully grafted, and stable particles of S-NH_2 with a small number of epoxy groups were retained in the MFCs after polymerization, owing to incomplete amination of S-GMA.

Fig. 6 shows the XPS data for MFCs-3 and MFCs-4. Signals of S, C, and O were clearly observed for MFCs-3 and MFCs-4 (Fig. 6a), indicating the presence of –SO_3H groups in the MFCs. Correspondingly, a peak around 284.3 eV, associated with the C–S bonds, was apparent in the C 1s XPS spectra of these catalysts (Fig. 6b). This result further proved the successful introduction of –SO_3H into the network of these samples, where the –SO_3H groups should increase the acid strength of these solid acids.[48] Moreover, the N 1s peak at 427.2 eV could be observed only for MFCs-3 (Fig. 6c), demonstrating that the S-NH_2 particles provided basic sites in the catalyst.

Fig. 7 shows the TG-DSC curves of S-GMA (a), S-NH_2 (b), MFCs-1 (c), MFCs-2 (d), MFCs-3 (e), and MFCs-4 (f). The TG profiles of all samples showed two distinct mass loss steps, and the corresponding DSC curves indicated endothermic or exothermic reactions based on the peak temperature (T_p). Initial weight losses of S-GMA (10.49%) and S-NH_2 (44.23%) were observed in the region of 25 °C to 250 °C because of dehydration, and the DSC curves also showed an endothermic

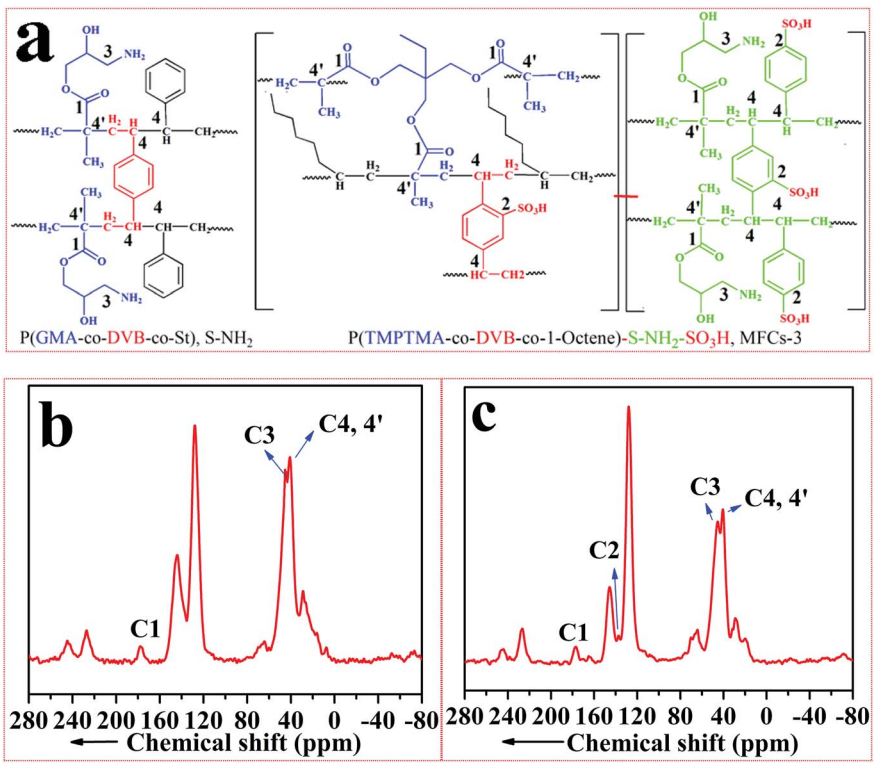

Fig. 5 The condensed structural formulas of S-NH_2 and MFCs-3 (a), and ^{13}C cross-polarization magic angle spinning (CP/MAS) NMR spectrum of S-NH_2 (b), and MFCs-3 (c).

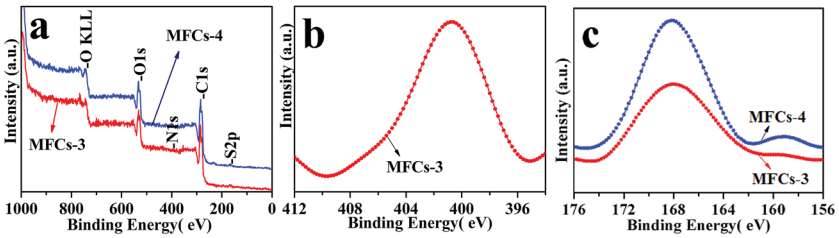

Fig. 6 X-ray photoelectron spectroscopy (XPS) measurements of survey (a), N 1s (b), and S 2p (c) of MFCs-3 and MFCs-4.

peak in the case of S-GMA (T_p = 99.8 °C) and S-NH_2 (T_p = 79.1 °C) in the same temperature range, suggesting that the hydrophilic –NH_2 groups were successfully grafted onto S-GMA and more water was captured by S-NH_2. The second major mass loss was observed between 250 °C and 750 °C for S-GMA (88.83%) and S-NH_2 (52.31%). The DSC curve of S-GMA showed two endothermic peaks (T_p = 269.6 °C and 437.4 °C), and the DSC curve of S-NH_2 showed one endothermic peak (T_p = 405.2 °C) that could be attributed to decomposition of the polymer network. The final residue from thermal decomposition of S-GMA and S-NH_2 may be litter carbon from calcination of the polymers, where the residue constituted about 0.68% and 3.46% of the respective initial masses. A peak indicative of slight weight loss and only one endothermic peak were observed for MFCs-1 (16.56%, T_p = 57.9 °C), MFCs-2 (17.73%, T_p = 60.6 °C), MFCs-3 (13.90%, T_p = 57.8 °C), and MFCs-4 (18.36%, T_p = 63.4 °C) within the initial temperature range (<250 °C for MFCs-2, MFCs-3, and MFCs-4, <300 °C for MFCs-1), which also may be derived from loss of H_2O from these samples.[49] Increasing the temperature to 800 °C resulted in significant weight loss and an exothermic peak was observed in the profile of MFCs-2 (66.57%, T_p = 508.7 °C), MFCs-3 (57.28%, T_p = 505.7 °C), and MFCs-4 (72.66%, T_p = 508.4 °C); significant weight loss and a large endothermic peak resulting from oxidation of organic matter (pyrolysis) and decomposition of –SO_3H groups[50] also was observed for MFCs-1 (55.76%, T_p = 463.4 °C). Furthermore, the TG-DSC curves of MFCs-2, MFCs-3, and MFCs-4 were similar, suggesting that the chemical composition and chemical structure of these species were similar. However, the TG-DSC curve of MFCs-1 was distinctly different from those of the other MFCs. Notably, sharp weight loss and a large endothermic peak were observed at about 463.4 °C in the case of MFCs-1. The difference in the TG-DSC curves may arise from MFCs-1 possessing less oxygen than the other MFCs, which contained the poly-TMPTMA component. Normally, when less oxygen is involved in the pyrolysis process, less energy is released during oxidation of the organic matter to gas. Nevertheless, the rapid decomposition of –SO_3H at around 463.4 °C required a significant amount of energy, resulting in the large endothermic peak and sharp weight loss of MFCs-1 at about 463.4 °C. The remaining mass of the catalysts at 800 °C may be residual carbon generated by calcination of the polymers.[51] Overall, it was found that the MFCs had high thermal stability, and the chemical composition and chemical structure of MFCs-1 were different from those of the other MFCs.

3.4 Acidic and basic properties of the catalysts

The approach presented herein is effective for synthesis of acid–base bi-functionalized catalysts, where the acidic and basic properties can be easily adjusted by controlling the contents of DVB and S-NH_2. The –SO_3H groups grafted onto the benzene ring of DVB offered acidity, whereas the S-NH_2 particles served multifunctional roles of stabilizing the emulsion and providing basic sites. The acid and base strengths of the MFCs were measured and classified based on CO_2-TPD and NH_3-TPD data (Fig. 8). These results provide reliable data based on the measurement principle even if the MFCs are degraded at high temperature. Using this technique, the test gas (CO_2 and NH_3) adsorbed on the active site of the MFCs can be totally desorbed at high temperature followed by analysis of the desorbed gas; no test gas (NH_3) was generated during degradation of the MFCs. Although it is likely that an acrylic polymer will release CO_2 when it decomposes, the content of acrylic groups in MFCs is very low. Also, based on the TPD measures under He environment, it is not possible that acrylic groups release only CO_2 when decomposing. In brief, as shown in Fig. 8, the MFCs all had different active site types with strong, middle, or weak strengths;[52] the number of acidic and basic sites was calculated as summarized in Table 3. The total amounts of acid and base were closely related to the contents of S (0.755 mmol g^{-1} for MFCs-1, 1.658 mmol g^{-1} for MFCs-2, 1.32 mmol g^{-1} for MFCs-3, and 1.293 mmol g^{-1} for MFCs-4) and N (0.480 mmol g^{-1} for MFCs-1, 0.662 mmol g^{-1} for MFCs-2, 0.735 mmol g^{-1} for MFCs-3, and 0 mmol g^{-1} for MFCs-4) in the MFCs (Table S1†), where these elements are derived from the volume of DVB and the amount of S-NH_2, respectively. Although MFCs-1 had the largest volume of DVB (2.0 mL) and the highest BET specific surface area (183.6 m^2 g^{-1}), the acid amount (0.769 mmol g^{-1}) was lower than that of the other catalysts (MFCs-2 with 1.732 mmol g^{-1}, MFCs-3 with 1.305 mmol g^{-1}, MFCs-4 with 1.332 mmol g^{-1}). This may be because the dense polymer network resulting from the highly cross-linked structure of TMPTMA and DVB[53] in MFCs-1 hindered grafting of the –SO_3H groups to the benzene ring of DVB during the sulfonation process. The total base contents of MFCs-1 (0.48 mmol g^{-1}), MFCs-2 (0.62 mmol g^{-1}), and MFCs-3 (0.735 mmol g^{-1}) were different. Kovačič's group found that stabilized nanoparticles were randomly embedded on the surface of macroporous polymers derived from Pickering HIPEs.[54] In this work, although the same amount of S-NH_2 was used to stabilize the emulsion, a possible reason for the difference in base contents of MFCs is that distinct amounts of

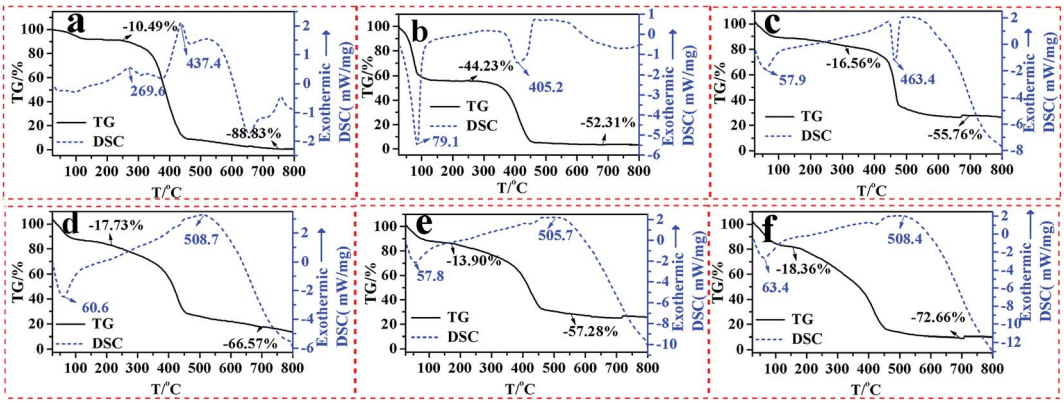

Fig. 7 TG-DSC curves of S-GMA (a), S-NH_2 (b), MFCs-1 (c), MFCs-2 (d), MFCs-3 (e), and MFCs-4 (f).

S-NH_2 were distributed into the catalysts per unit mass. Furthermore, there was only N in the unsulfonated MFCs-3 (0.894 mmol g^{-1} of N and 0.873 mmol g^{-1} of basicity, Table S1 and S4†), which further demonstrated that the sulfonation process has no effect on the base amount of catalyst, and the fact that S was introduced into MFCs by the sulfonation process. Thus, the acid–base properties of the MFCs can be easily adjusted by controlling the volume of DVB and the amount of S-NH_2, thereby offering a simple method for manipulation of the acid–base strength of polymeric catalysts.

3.5 Conversion of cellulose to HMF

In general, thermal stability of catalysts is very important for their practical applications in catalytic reactions. Although TG analysis of the MFCs indirectly indicated strong thermal stability of the catalysts, it is necessary to confirm whether the thermal stability of the MFCs meets the requirements for conversion of cellulose to HMF. Thus, MFCs-3 was further treated for 5.0 h at 200 °C, which exceeds the highest reaction temperature of 150 °C. The SEM image in Fig. S5† shows that heat-treated MFCs-3 possessed stable macropores with a well-defined, open-cell and interconnected pore throat structure, which was similar to that of as-produced MFCs-3. ESI-MS spectra (Fig. S6†) and FT-IR spectra (Fig. S7†) of the solution were largely similar before and after solution treatment when MFCs-3 powder (50 mg) was added to hexadecane (2.0 g) or [EMIM]-Cl (2.0 g) at 150 °C for 5.0 h under stirring, suggesting that MFCs-3 had high thermal stability and that there was no leaching of the acidic and basic groups of MFCs-3 in the reaction medium. The practical use of the MFCs for catalytic conversion of cellulose to HMF was investigated. To ensure the use of optimal reaction conditions, MFCs-3 was used as a representative MFC catalyst. The influence of the catalyst loading on the catalytic activity is summarized in Fig. 9a. Increasing the catalyst loading from 20 mg to 40 mg induced a gradual increase of the HMF yield to reach a maximum of 41% at a loading of 40 mg. A further increase in the catalyst loading decreased the yield, indicating that the decomposition side reaction or polymerization of HMF was enhanced with high catalyst loading.[55] Using the optimized catalyst loading of 40 mg, the effects of reaction temperature and time were evaluated on conversion of cellulose into HMF, as shown in Fig. 9b. The

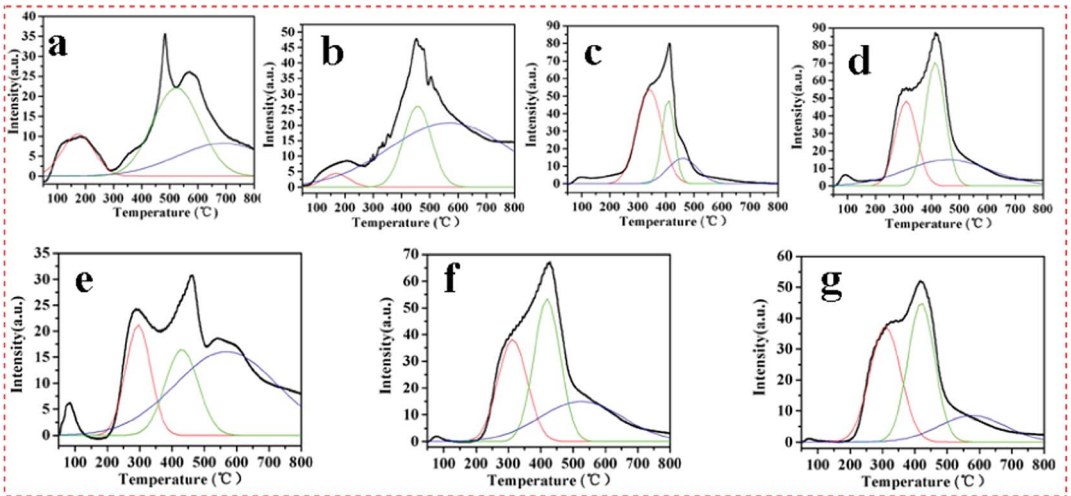

Fig. 8 NH_3-TPD curves of MFCs-1 (a), MFCs-2 (b), MFCs-3 (c), MFCs-4 (d), and CO_2-TPD curves of MFCs-1 (e), MFCs-2 (f), MFCs-3 (g).

Table 3 Acidic and basic properties of the MFCs

Samples	Acid strength (°C)	Acid amounts (mmol g^{-1})	Total acidity (mmol g^{-1})	Base strength (°C)	Base amounts (mmol g^{-1})	Total basicity (mmol g^{-1})
MFCs-1	168	0.119	0.769	297	0.094	0.480
	528	0.376		426	0.096	
	694	0.274		567	0.290	
MFCs-2	168	0.058	1.732	311	0.196	0.662
	450	0.380		420	0.248	
	566	1.294		528	0.218	
MFCs-3	335	0.740	1.305	309	0.291	0.735
	412	0.330		425	0.302	
	463	0.235		579	0.142	
MFCs-4	309	0.370	1.332	0	0	0
	412	0.504				
	450	0.458				

HMF yield increased rapidly during the initial period, then decreased with progression of the reaction time. An appropriate combination of reaction temperature and reaction time can be used to obtain the maximum HMF yield (*i.e.*, 110 °C and 180 min for 35.5%, 120 °C and 60 min for 41.0%, 130 °C and 20 min for 42.2%, 140 °C and 20 min for 30.1%). It is possible that elevation of the reaction temperature reduced the viscosity of the ionic liquids thereby enhancing the catalyst activity; this could accelerate degradation of cellulose to HMF, but simultaneously increased the formation of by-products, including unidentified soluble polymers and insoluble compounds that covered the active sites of the catalysts. Zakrzewska also reported similar results where HMF was decomposed into unidentified products at high temperature.[56] Overall, the optimal yield of HMF was obtained with MFCs-3 (41%) at a catalyst loading of 40 mg, a reaction time of 60 min, and a temperature of 120 °C.

The influences of wettability, acid–base strength, and the hierarchical porous properties of the MFCs on the HMF yield were further studied. Under the optimal reaction conditions determined above using MFCs-3, the yields of HMF obtained with MFCs-1, MFCs-2, MFCs-3, and MFCs-4 were 27.1%, 30.1%, 41%, and 33.5%, respectively (Fig. 10). The yield of HMF obtained with MFCs-4 was lower than that obtained with MFCs-3 owing to the lack of basic sites. However, hydrophobic MFCs-4 with a low BET specific surface area still gave rise to a higher yield of HMF than that obtained with hydrophilic MFCs-1 with a high BET specific surface area and basic sites. Additionally, the more hydrophobic MFCs-3 also gave rise to a higher yield of HMF than that obtained with MFCs-2 with a higher BET specific surface area and acid–base strength. Thus, it could be concluded that the hydrophobic surface and the basic sites contributed to the excellent performance of the MFCs, rather than the proper BET specific surface area and acid strength.[57] The HMF yield was affected by these factors in the following order: surface hydrophobicity > acid–base bi-functionality > acid strength > hierarchical porous structure > mesoporous structure, which can be explained as follows. Firstly, the basic sites promote isomerization of glucose to fructose. Secondly, a hydrophobic surface is more conducive to curtailing side reactions of HMF that generate other by-products. Thirdly, a higher yield of HMF (33.5%) was obtained with MFCs-4 having a hierarchical porous structure than obtained with acidic silica nanoparticles with a strictly mesoporous structure (10%),[58] suggesting that the hierarchical porous structure was advantageous for conversion of cellulose to HMF. To discuss the effect of adsorption of a certain amount of water and/or solvents by the polymeric foams prior to the catalytic experiments on the catalytic reaction, a small amount of additional water was introduced into the reaction medium during the catalytic reaction under the same reaction conditions as employed for MFCs-3. Interestingly, although this additional water was most probably released into the reaction medium during catalysis, the HMF yield (41.3%) was similar to that obtained with MFCs-3 (41%) without addition of water, suggesting that a little adsorbed water in the catalyst had no influence on the HMF yield.

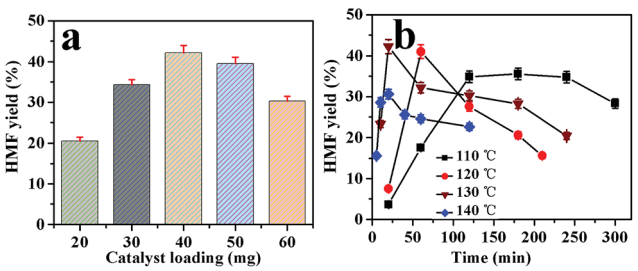

Fig. 9 Effect of catalyst loading (a) with reaction conditions: 130 °C, 20 min, 100 mg cellulose, 2.0 g [BMIM]Cl, and the effects of reaction temperature and time (b) with reaction conditions: 40 mg MFCs-3, 100 mg cellulose, 2.0 g [BMIM]Cl on the conversion of cellulose into HMF by MFCs-3 as catalyst, respectively.

3.6 Reusability and characterization of reused MFCs-3

The reusability of the catalyst is very important for practical production of HMF in accord with demands for green and sustainable chemistry. Regeneration tests were conducted under the optimized reaction conditions, and the HMF yield after four reaction cycles (41.3% ± 2.1, 40.1% ± 2.0, 38.4% ± 1.98, and 35.2% ± 1.76 for successive cycles) is shown in

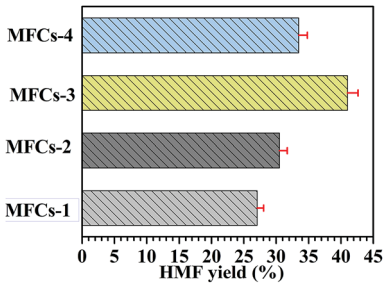

Fig. 10 Dehydration of cellulose by different catalyst reaction conditions: 40 mg catalysts, 120 °C, 60 min, 100 mg cellulose, and 2.0 g [BMIM]Cl.

Fig. 11a. MFCs-3 was readily recovered by simply filtering the mixture at the end of the first reaction cycle, washing copiously with a mixture of *n*-hexane and methanol, and drying at 30 °C for 24 h in a vacuum oven. The pH of the transparent filtrate was near neutral, indirectly suggesting that there was no leaching of the acidic and basic groups into the reaction medium during catalysis. The recovered MFCs-3 was used to catalyze the conversion of cellulose to HMF over four successive cycles, and MFCs-3 recovered after the fourth cycle was again characterized by elemental analysis, NH_3-TPD, CO_2-TPD, XPS, and SEM. The total amounts of acid and base (1.2 mmol g^{-1} of acid, 0.64 mmol g^{-1} of base) and the elemental compositions of S and N (2.77% and 1.179 mmol g^{-1} of S, 0.63% and 0.582 mmol g^{-1} of N) (Fig. 11b and Table S1†) declined only slightly compared with the corresponding values for as-prepared MFCs-3 (1.305 mmol g^{-1} of acid, 0.735 mmol g^{-1} of base, 6.77% and 1.32 mmol g^{-1} of S, 1.22% and 0.782 mmol g^{-1} of N), suggesting only a slight loss of the acid and base sites of the catalysts after repeated catalytic cycles. Furthermore, the MFCs-3 catalyst still retained excellent activity after four reaction cycles. Moreover, N and S peaks were still detected in the XPS spectra of MFCs-3 recovered after the fourth cycle (Fig. 11c), and the rigid porous structure also could be observed from the SEM image (Fig. 11d), indicating that MFCs-3 possesses superior recyclability and reusability with high mechanical stability of the polymer network, as well as excellent chemical stability of the acidic and basic sites. These results suggest that the heterogeneous MFCs-3 catalyst has potential for application in practical production of HMF.

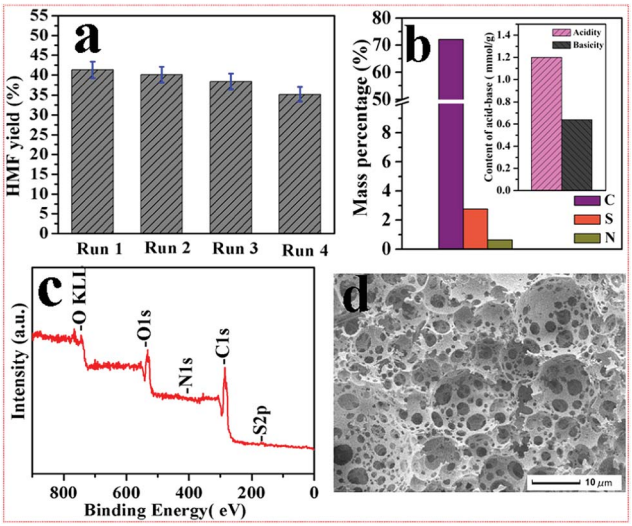

Fig. 11 Reusability of MFCs-3 catalyst in the dehydration of cellulose into HMF in [EMIM]Cl under the optimized conditions: 120 °C, 40 mg of catalyst based on 0.10 g of cellulose, 60 min, 2.0 g [EMIM]Cl (a), element contents (inset: contents of acid–base) (b), XPS measurements of survey (c), and SEM image (d) of MFCs-3 recovered after the fourth cycle.

4 Conclusion

In summary, we prepared a series of adjustable hydrophobic, acid–base and hierarchical porous microcellular foam catalysts using a Pickering HIPEs template method. The wettability, acid–base and hierarchical porous structure of the MFCs could be adjusted easily *via* changes to contents of DVB, TMPTMA, 1-octene monomer and S-NH_2 nanoparticles, respectively. The high HMF yield (41%) was achieved by a one-pot catalyzed conversion of cellulose to HMF with MFCs-3, and it was confirmed that the hydrophobic surface had more advantageous influence than BET specific surface area, acid–base and hierarchical porous structure for conversion of cellulose to HMF. This work opens up a route to produce multifunctional polymeric catalysts for efficient one-pot conversion of cellulose to HMF.

Acknowledgements

This work was financially supported by the National Natural Science Foundation of China (no. 21107037, no. 21176107, no. 21306013, no. 21203079, no. 21407064, no. 21203079), Natural Science Foundation of Jiangsu Province (no. BK20131223), National Postdoctoral Science Foundation (no. 2013M530240), Special National Postdoctoral Science Foundation (no. 2014T70480), Postdoctoral Science Foundation of Jiangsu Province (no. 1202002B), Doctoral Innovation Fund of Jiangsu University of Science and Technology (no. 635211202) and Programs of Senior Talent Foundation of Jiangsu University (no. 12JDG090).

References

1 L. Q. Wu, J. L. Song, B. B. Zhang, B. W. Zhou, H. C. Zhou, H. L. Fan, Y. Y. Yang and B. X. Han, *Green Chem.*, 2014, **16**, 3935–3941.
2 L. Bromberg, X. Su and T. A. Hatton, *Chem. Mater.*, 2014, **26**, 6257–6264.
3 M. G. Mazzotta, D. Gupta, B. Saha, A. K. Patra, A. Bhaumik and M. M. Abu-Omar, *ChemSusChem*, 2014, **7**, 2342–2350.
4 P. Lanzafame, G. Centi and S. Perathoner, *Chem. Soc. Rev.*, 2014, **43**, 7562–7580.
5 S. Dutta and M. Mascal, *ChemSusChem*, 2014, **7**, 3028–3030.
6 Y. H. Zu, P. P. Yang, J. J. Wang, X. H. Liu, J. W. Ren, G. Z. Lu and Y. Q. Wang, *Appl. Catal., B*, 2014, **146**, 244–248.

7 Y. B. Huang, M. Y. Chen, L. Yan, Q. X. Guo and Y. Fu, *ChemSusChem*, 2014, **7**, 1068–1072.
8 X. Y. Wan, C. M. Zhou, J. S. Chen, W. P. Deng, Q. H. Zhang, Y. H. Yang and Y. Wang, *ACS Catal.*, 2014, **4**, 2175–2185.
9 S. Albonetti, A. Lolli, V. Morandi, A. Migliori, C. Lucarelli and F. Cavani, *Appl. Catal., B*, 2015, **163**, 520–530.
10 M. Besson, P. Gallezot and C. Pinel, *Chem. Rev.*, 2014, **114**, 1827–1870.
11 B. Danon, G. Marcotullio and W. de Jong, *Green Chem.*, 2014, **16**, 39–54.
12 M. A. Mellmer, C. Sener, J. M. R. Gallo, J. S. Luterbacher, D. M. Alonso and J. A. Dumesic, *Angew. Chem., Int. Ed.*, 2014, **53**, 11872–11875.
13 J. M. R. Gallo, J. S. Luterbacher, D. M. Alonso, M. A. Mellmer and J. A. Dumesic, *Green Chem.*, 2013, **15**, 85–90.
14 P. Lanzafame, D. M. Temi, S. Perathoner, A. N. Spadaro and G. Centi, *Catal. Today*, 2012, **179**, 178–184.
15 H. P. Gao, Y. X. Peng, J. M. Pan, J. Zeng, C. H. Song, Y. L. Zhang, Y. S. Yan and W. D. Shi, *RSC Adv.*, 2014, **4**, 43029–43038.
16 Y. L. Zhang, J. M. Pan, Y. S. Yan, W. D. Shi and L. B. Yu, *RSC Adv.*, 2014, **4**, 23797–23806.
17 Y. L. Yang, Z. T. Du, J. P. Ma, F. Lu, J. J. Zhang and J. Xu, *ChemSusChem*, 2014, **7**, 1352–1356.
18 F. J. Liu, W. P. Kong, C. Qi, L. F. Zhu and F. S. Xiao, *ACS Catal.*, 2012, **2**, 565–572.
19 L. Wang, H. Wang, F. J. Liu, A. M. Zheng, J. Zhang, Q. Sun, J. P. Lewis, L. F. Zhu, X. G. Meng and F. S. Xiao, *ChemSusChem*, 2014, **7**, 402–406.
20 W. H. Peng, Y. Y. Lee, C. Wu and K. C. W. Wu, *J. Mater. Chem.*, 2012, **22**, 23181–23185.
21 X. Gao, X. Q. Zou, H. P. Ma, S. Meng and G. S. Zhu, *Adv. Mater.*, 2014, **26**, 3644–3648.
22 J. P. Alper, S. Wang, F. Rossi, G. Salviati, N. Yiu, C. Carraro and R. Maboudian, *Nano Lett.*, 2014, **14**, 1843–1847.
23 E. Slovakova, M. Jeselnik, E. Zagar, J. Zednik, J. Sedlacek and S. Kovacic, *Macromolecules*, 2014, **47**, 4864–4869.
24 Z. J. Wang, S. Ghasimi, K. Landfester and K. A. I. Zhang, *J. Mater. Chem. A*, 2014, **2**, 18720–18724.
25 W. J. Jiang, C. M. Grozea, Z. Q. Shi and G. J. Liu, *ACS Appl. Mater. Interfaces*, 2014, **6**, 2629–2638.
26 H. Huang, C. A. Denard, R. Alamillo, A. J. Crisci, Y. R. Miao, J. A. Dumesic, S. L. Scott and H. M. Zhao, *ACS Catal.*, 2014, **4**, 2165–2168.
27 Y. Zhu, S. M. Zhang, Y. Hua, J. D. Chen and C. P. Hu, *Polymer*, 2010, **51**, 3612–3617.
28 Y. Hu, X. Y. Gu, Y. Yang, J. Huang, M. Hu, W. Chen, Z. Tong and C. Y. Wang, *ACS Appl. Mater. Interfaces*, 2014, **6**, 17166–17175.
29 M. Destribats, B. Faure, M. Birot, O. Babot, V. Schmitt and R. Backov, *Adv. Funct. Mater.*, 2012, **22**, 2642–2654.
30 B. Neirinck, J. Fransaer, O. V. Biest and J. Vleugels, *J. Eur. Ceram. Soc.*, 2009, **29**, 833–836.
31 V. O. Ikem, A. Menner and A. Bismarck, *Angew. Chem., Int. Ed.*, 2008, **47**, 8277–8279.
32 N. R. Cameron, *Polymer*, 2005, **46**, 1439–1449.
33 A. Menner, R. Powell and A. Bismarck, *Macromolecules*, 2006, **39**, 2034–2035.
34 A. Menner, K. Haibach, R. Powell and A. Bismarck, *Polymer*, 2006, **47**, 7628–7635.
35 S. S. Manley, N. Graeber, Z. Grof, A. Menner, G. F. Hewitt, F. Stepanek and A. Bismarck, *Soft Matter*, 2009, **5**, 4780–4787.
36 V. O. Ikem, A. Menner, T. S. Horozov and A. Bismarck, *Adv. Mater.*, 2010, **22**, 3588–3592.
37 M. S. Silverstein, *Prog. Polym. Sci.*, 2014, **39**, 199–234.
38 N. R. Cameron, D. C. Sherrington, L. Albiston and D. P. Gregory, *Colloid Polym. Sci.*, 1996, **274**, 592–595.
39 X. H. Zheng, Y. Zhang, H. T. Wang and Q. G. Du, *Macromolecules*, 2014, **47**, 6847–6855.
40 J. M. Pan, Q. Qu, J. Cao, D. Yan, J. X. Liu, X. H. Dai and Y. S. Yan, *Chem. Eng. J.*, 2014, **253**, 138–147.
41 F. Zhang, C. Liang, X. T. Wu and H. X. Li, *Angew. Chem., Int. Ed.*, 2014, **53**, 8498–8502.
42 L. Chen, G. Zhu, D. Zhang, H. Zhao, M. Guo, W. Shi and S. Qiu, *J. Mater. Chem.*, 2009, **19**, 2013–2017.
43 D. C. Niu, Z. J. Liu, Y. S. Li, X. F. Luo, J. Y. Zhang, J. P. Gong and J. L. Shi, *Adv. Mater.*, 2014, **26**, 4947–4953.
44 A. Dutta, D. Gupta, A. K. Patra, B. Saha and A. Bhaumik, *ChemSusChem*, 2014, **7**, 925–933.
45 A. Vílchez, C. Rodríguez-Abreu, A. Menner, A. Bismarck and J. Esquena, *Langmuir*, 2014, **30**, 5064–5074.
46 Y. Yang, X. Liu, X. B. Li, J. Zhao, S. Y. Bai, J. Liu and Q. H. Yang, *Angew. Chem., Int. Ed.*, 2012, **51**, 9164–9168.
47 D. C. Niu, Z. J. Liu, Y. S. Li, F. Luo, J. Y. Zhang, J. P. Gong and J. L. Shi, *Adv. Mater.*, 2014, **29**, 4947–4953.
48 P. A. Russo, M. M. Antunes, P. Neves, P. V. Wiper, E. Fazio, F. Neri, F. Barreca, L. Mafra, M. Pillinger, N. Pinna and A. A. Valente, *J. Mater. Chem. A*, 2014, **2**, 11813–11824.
49 L. Wang, H. Wang, F. J. Liu, A. M. Zheng, J. Zhang, Q. Sun, J. P. Lewis, L. F. Zhu, X. J. Meng and F. S. Xiao, *ChemSusChem*, 2014, **7**, 402–406.
50 R. Jia, J. W. Ren, X. H. Liu, G. Z. Lu and Y. Q. Wang, *J. Mater. Chem. A*, 2014, **2**, 11195–11201.
51 J. M. Pan, B. Wang, J. D. Dai, X. H. Dai, H. Hang, H. X. Ou and Y. S. Yan, *J. Mater. Chem.*, 2012, **22**, 3360–3369.
52 R. D. Zhang, P. X. Li, N. Liu, W. R. Yue and B. H. Chen, *J. Mater. Chem. A*, 2014, **2**, 17329–17340.
53 M. Saleh, H. M. Lee, K. C. Kemp and K. S. Kim, *ACS Appl. Mater. Interfaces*, 2014, **6**(10), 7325–7333.
54 S. Kovačič, A. Anžlovar, B. Erjavec, G. Kapun, N. B. Matsko, M. Žigon, E. Žagar, A. Pintar and C. Slugovc, *ACS Appl. Mater. Interfaces*, 2014, **6**, 19075–19081.
55 M. G. Mazzotta, D. Gupta, B. Saha, A. K. Patra, A. Bhaumik and M. M. Abu-Omar, *ChemSusChem*, 2014, **7**, 2342–2350.
56 M. E. Zakrzewska, E. Bogel-Lukasik and R. Bogel-Lukasik, *Chem. Rev.*, 2011, **111**, 397–417.
57 J. Tuteja, H. Choudhary, S. Nishimura and K. Ebitani, *ChemSusChem*, 2014, **7**, 96–100.
58 W. H. Peng, Y. Y. Lee, C. Wu and K. C. W. Wu, *J. Mater. Chem.*, 2012, **22**, 23181–23185.

